

The dynamics of arsenic in saturated porous media: fate and transport modeling for deep aquatic sediments, wetland sediments, and groundwater environments

PETER R. JAFFE*, SOOKYUN WANG, PETER L. KALLIN¹, AND SHERWOOD L. SMITH²

Department of Civil and Environmental Engineering, Princeton University, Princeton, NJ 08544, USA

¹Now at OMNI Environmental Corporation, Princeton, NJ, USA

²Now at Frontier Research Program for Global Change SEAVANS, Tokyo, Japan

*Corresponding author. E-mail: jaffe@princeton.edu

Abstract—The fate and transport of many trace metals, metalloids, and radionuclides in porous media is closely linked to the biogeochemical reactions that occur as a result of organic carbon being sequentially degraded by different microorganisms using a series of terminal electron acceptors. The spatial distribution of these biogeochemical reactions is affected by processes that are often unique to and/or characteristic of a specific environment. We have developed a generic model formulation and applied it to simulate the fate and transport of arsenic in three distinct hydrologic settings, namely deep aquatic sediments (no rooted plants), wetland sediments, and groundwaters. The key differences in physical processes that have been considered are sedimentation, roots and their effects on biogeochemistry and advective transport, and differences in mixing processes. Steady-state formulations were applied to the sedimentary environments while a time-dependent formulation was applied to the groundwater case. Results of numerical simulations show that these physical processes significantly affect the chemical profiles of different electron acceptors, their reduced species, and arsenate as well as arsenite that will result from the degradation of an organic carbon source in the sediments or groundwater. Even though specific biological transformations are allowed to proceed only in zones where they are thermodynamically favorable, results show that mixing as well as abiotic reactions can make the profiles of individual electron acceptors overlap and/or appear to reverse their expected order.

1. INTRODUCTION

The fate and transport of many trace metals, metalloids, and radionuclides in porous media are closely linked to the biogeochemical reactions that occur as a result of organic carbon being degraded by different microorganisms using a series of terminal electron acceptors. Throughout the redox profile that develops in such environments, trace metals can be mobilized/immobilized via processes such as reduction/oxidation, sorption/desorption, precipitation/dissolution, and/or the formation of complex ions. Although the work presented here is generic and applies to a wide range of trace metals, metalloids, and radionuclides, for this study, we will focus the simulations specifically on arsenic as a model contaminant.

Arsenic is a ubiquitous contaminant that is, among others, associated with the chemical and power industry, as well as agriculture. The predominant forms of arsenic in natural water systems are As(V) as H_3AsO_4 (arsenate), and As(III) as H_3AsO_3 (arsenite). Arsenate is dominant in oxic waters, but under reducing conditions is converted to arsenite (Massacheleyn et al., 1991). Like phosphate, arsenate exists mainly in its deprotonated forms at natural pH

levels, and is therefore readily sorbed onto positively charged surfaces of minerals such as Fe(III) oxides (Fendorf et al., 1997; Dzombak and Morel, 1990). Bacteria have been identified which, in environments that are more reducing than nitrate reduction, can use arsenate as a terminal electron acceptor, reducing it to arsenite (Newman et al., 1997 a,b; Dowdle et al. 1996). Arsenite is the more toxic form of arsenic, and it exists primarily as a neutral dissolved species at ambient pH values, in zones that have a more reducing environment. Compared to arsenate, transport of arsenite is therefore not significantly retarded due to sorption (Gulens et al., 1979; Holm et al., 1979; Oscarson et al., 1980), but it has a high affinity to form complexes with sulfides, forming sulfide minerals such as orpiment (As_2S_3).

Given that the transport and bioavailability of many metals and metalloids are affected by similarly complex sets of chemical reactions and physical mechanisms, we have developed a general analytical framework to improve our understanding of how the fate and transport of these metals are affected by various biogeochemical and physical transport processes. Because these processes are highly environmentally dependent, the biogeochemical dynamics of arsenic

will be different in various environmental settings. In our simulations, we will focus on three important, permanently saturated, hydrologic settings, where redox conditions can range from highly oxidized to highly reduced, namely: deep aquatic sediments without rooted plants (referred to hereafter as deep sediments), wetland sediments with rooted macrophytes, and groundwaters. Our objective is to assess the main differences in model development as well as arsenic fate and transport in these environments.

Common to the modeling approach is that, distinct redox zones will develop as a result of the biodegradation of organic matter and the sequential utilization of different terminal electron acceptors, as shown in Table 1. The spatial distribution of these zones will determine where arsenic is reduced/oxidized, sorbed to different solid phases, and/or precipitates. Clearly pH is a key parameter in determining the fate of arsenic and other chemical constituents in the environments, and spatial/temporal pH values will depend on the different biotic and abiotic reactions occurring in each redox zone. Complex microbial and chemical redox reactions could change pH conditions in the aquatic system by producing/consuming acid and base constituents during the decomposition of organic matter. For the purpose of this work, however, pH will be considered a model input and will not be simulated explicitly.

1.1. Differences in Model Formulations between Deep Sediments, Wetland Sediments, and Groundwater.

A fundamental difference between saturated sediments near the sediment/water interface (deep and wetland sediments) and in the subsurface (groundwater environments) is that, at the interface, sedimentation provides a source for new and usually oxidized sediments. This is important, in that this sedimentation process normally provides a source of fresh iron and manganese oxides. Thus, in sedimentary environments, a quasi-steady-state spatial profile can develop containing a reacting solid phase of Mn(IV) and/or Fe(III). In a system where the solid phase is stationary, such as groundwaters, steady-state conditions cannot result in the presence of such reacting solid phases. It should be noted that only a fraction of the Mn(IV) and Fe(III) is bioavailable. Amorphous iron oxide may be bioavailable while crystalline forms are not. To simulate biogeochemical dynamics in groundwater environments where the bioavailable fraction of Mn(IV) and Fe(III) are being consumed as terminal electron acceptors, one needs to use non-steady-state models that can simulate the profiles of these species over space and time.

For deep and wetland sediments, an oxidized surface layer of sediment is typically present at the sediment/water interface (Gambrell and Patrick, 1978; Ponnampuruma, 1984; Mitsch and Gosselink, 1993), which is followed by a steep redox gradient, resulting from the different reactions shown in Table 1 proceeding sequentially. Concentration gradients of redox species of more than an order of magnitude over a distance of a centimeter have been observed in different sediments (Brendel and Luther, 1995). Because of much lower total bioavailable organic carbon in groundwater environments, and often higher water-flow velocities, these same redox gradients occur over significantly longer distances in these settings (Hunter et al., 1998).

Arsenic may be immobilized due to sorption onto different organic and inorganic soil constituents, or due to precipitation. Adsorption of arsenate onto iron and manganese oxides is an important process where the oxidation potential is high. As the system becomes more reduced, iron and manganese oxides are depleted, and trace metals, as well as arsenic, can desorb and remobilize as a dissolved species, although in the presence of sulfide ions, are usually immobilized as sulfides.

In addition to the processes described above, redox profiles in wetland sediments are also affected by the presence of higher plants. Wetland plants have evolved specialized adaptations to supply oxygen to the roots, and to transfer oxygen from the roots into the surrounding sediment (Armstrong, 1979; Sand-Jensen et al., 1982; Bedford et al., 1991; Mendelsohn, 1993). This transfer of oxygen maintains an oxidizing potential in the rhizosphere, which is important for root survival. It protects roots from phytotoxins, which are common in swamps at low redox potentials, and prevents transport into the root of highly soluble Fe(II) ions by precipitating them at the root surface following oxidation to Fe(III) (Grosse, 1997). The rates of oxygen transfer into wetland sediments can be substantial and highly variable (Armstrong, 1979; Bedford et al., 1991; Brix, 1993; Sorrel, 1994). These rates are dependent on the type of vegetation and root size, as well as the chemical composition and oxygen demand of the sediments (Brix et al., 1996). Oxygen release rates measured for *E. sphacelata* ranged from non-detection for roots placed in a deoxygenated solution, to $55 \mu\text{mol h}^{-1} \text{g}^{-1}$ dry weight when placed in a solution with a redox potential of -200 mV (Sorrel et al., 1993). The degree of iron plaque accumulation on roots is highly variable, and depends on the concentration of ferrous iron in solution as well as its complexation with organic ligands and the availability of other exchange sites on different soil mineral and organic fractions

Table 1. Key biogeochemical model stoichiometric relationships.

Layer	Stoichiometric relationships for the major model redox reactions ¹
1.	$(\text{CH}_2\text{O})_{106}(\text{NH}_3)_{16}(\text{H}_3\text{PO}_4) + 106 \text{O}_2 \rightarrow 106 \text{CO}_2 + 16 \text{NH}_3 + \text{H}_3\text{PO}_3 + 106 \text{H}_2\text{O}$ a. $\text{NH}_4^+ + 2 \text{O}_2 \rightarrow \text{NO}_3^- + \text{H}_2\text{O} + 2 \text{H}^+$ b. $2 \text{Mn}^{2+} + \text{O}_2 + 2 \text{H}_2\text{O} \rightarrow 2 \text{MnO}_2 + 4 \text{H}^+$ c. $4 \text{Fe}^{2+} + \text{O}_2 + 10 \text{H}_2\text{O} \rightarrow 4 \text{Fe}(\text{OH})_3 + 8 \text{H}^+$ d. $\text{H}_2\text{S} + 2 \text{O}_2 \rightarrow \text{SO}_4^{2-} + 2 \text{H}^+$ e. $\text{CH}_4 + 2 \text{O}_2 \rightarrow \text{CO}_2 + 2 \text{H}_2\text{O}$
2.	$(\text{CH}_2\text{O})_{106}(\text{NH}_3)_{16}(\text{H}_3\text{PO}_4) + 84.8 \text{NO}_3^- + 84.8 \text{H}^+ \rightarrow 106 \text{CO}_2 + 42.4 \text{N}_2 + 16 \text{NH}_3 + \text{H}_3\text{PO}_3 + 148.4 \text{H}_2\text{O}$
3.	$(\text{CH}_2\text{O})_{106}(\text{NH}_3)_{16}(\text{H}_3\text{PO}_4) + 212 \text{MnO}_2 + 424 \text{H}^+ \rightarrow 106 \text{CO}_2 + 212 \text{Mn}^{2+} + 16 \text{NH}_3 + \text{H}_3\text{PO}_3 + 318 \text{H}_2\text{O}$ a. $\text{MnO}_2 + \text{H}_2\text{S} + 2 \text{H}^+ \rightarrow \text{Mn}^{2+} + \text{S}^0 + 2 \text{H}_2\text{O}$ b. $\text{MnO}_2 + 2 \text{Fe}^{2+} + 4 \text{H}_2\text{O} \rightarrow \text{Mn}^{2+} + 2 \text{Fe}(\text{OH})_3 + 2 \text{H}^+$
4.	$(\text{CH}_2\text{O})_{106}(\text{NH}_3)_{16}(\text{H}_3\text{PO}_4) + 424 \text{FeOOH} + 848 \text{H}^+ \rightarrow 106 \text{CO}_2 + 424 \text{Fe}^{2+} + 16 \text{NH}_3 + \text{H}_3\text{PO}_3 + 742 \text{H}_2\text{O}$ a. $2 \text{Fe}(\text{OH})_3 + \text{H}_2\text{S} + 4 \text{H}^+ \rightarrow 2 \text{Fe}^{2+} + \text{S}^0 + 6 \text{H}_2\text{O}$
5.	$(\text{CH}_2\text{O})_{106}(\text{NH}_3)_{16}(\text{H}_3\text{PO}_4) + 53 \text{SO}_4^{2-} + 53 \text{H}^+ \rightarrow 106 \text{CO}_2 + 53 \text{HS}^- + 16 \text{NH}_3 + \text{H}_3\text{PO}_3 + 106 \text{H}_2\text{O}$ a. $\text{SO}_4^{2-} + \text{CH}_4 + 2 \text{H}^+ \rightarrow \text{H}_2\text{S} + \text{CO}_2 + 2 \text{H}_2\text{O}$
6.	$(\text{CH}_2\text{O})_{106}(\text{NH}_3)_{16}(\text{H}_3\text{PO}_4) \rightarrow 53 \text{CO}_2 + 53 \text{CH}_4 + 16 \text{NH}_3 + \text{H}_3\text{PO}_4$

¹ In these reactions, the organic material is represented by the Redfield stoichiometry, which differs for terrestrial ecosystems (Vitousek et al., 1988), and can be adjusted depending on the characteristics of the sediment organic carbon source, wetland litter, or carbon source injected into the subsurface. To facilitate comparison between the simulations, the same carbon formulation was used in all cases. It should also be noted that sulfur is not included in the Redfield formula and that therefore the sulfur source used here is external from the organic matter.

(Mendelsohn, 1993). Adsorption of arsenic, as well as other trace metals, can be significantly enhanced in the rhizosphere due to the formation of these iron oxyhydroxide plaques on roots (Otte et al., 1995). In addition to oxygen transfer, evapotranspiration also affects the redox profile of wetland sediments, by inducing advection that changes the vertical flow velocity profile.

1.2. Simulation of the Dynamics of Trace Metals and Metalloids in Saturated Porous Media.

Biologically-mediated redox dynamics in fresh- and marine water sediments, as well as groundwaters, have been simulated in terms of the sequential utilization of different electron acceptors during the biodegradation of sediment organic matter (Rabouille and Gaillard, 1991; Sweerts et al., 1991; Matsunaga et al., 1993; Van Cappellen and Wang, 1995; Dhakar and Burdige, 1996; Park and Jaffé, 1996; Wang and Van

Cappellen, 1996; Hunter et al., 1998). Based on these biogeochemical processes, trace-metal dynamics in groundwater have been described by several authors (e.g., Egesgaard and Kipp, 1992; Lensing et al., 1994; Yeh and Tripathi, 1991). In many of these studies, it was assumed that the metal is at equilibrium with the surrounding geochemistry. Clearly this is not always the case. Fe(II) for example, can be found in measurable amounts in oxic and nitrate-reducing waters, where it has been transported from zones where Fe(III) is being reduced. Non-equilibrium conditions have therefore been implemented in formulating the cycling of iron and manganese by many of these investigators (e.g., Hunter et al., 1998), and for contaminant trace metals that undergo redox reactions where the metals are kinetically driven towards chemical equilibrium by biological reactions (Smith and Jaffé, 1998) or abiotic reduction (Jardine et al., 1999).

In this work, we will use the same biogeochemical formulations for the three environmental settings being compared. The fundamentals of the model for-

mulation and required modifications for deep sediments, wetland sediments, and groundwaters are described below. The generic equations are given in the Appendix, and a detailed description of the model implementation for sediments is given in Smith and Jaffé, (1998). The spatial (vertical in sediments, and horizontal in groundwater) profiles of fifteen coupled constituents, including solid (organic matter, manganese oxides, iron oxides, and orpiment) and dissolved substances (dissolved organic carbon, oxygen, nitrate, sulfate, ammonia, dissolved manganese, dissolved iron, sulfide, methane, arsenate, and arsenite), and their interactions, including phase changes such as precipitation, dissolution, and sorption, are described.

To model the profile of the redox conditions in saturated porous media, we describe the degradation of organic matter and the sequential reduction of electron acceptors, taking into account where appropriate, transport processes such as molecular diffusion, dispersion, bioturbation, irrigation, and advection. Bioturbation and irrigation are described as a mixing process similar to dispersion and molecular diffusion, as discussed by Berner (1980). Bioturbation and irrigation are processes driven by benthic organisms, which are present in deep sediments and wetland sediments, but are absent in groundwater environments. Based on the electron acceptor that is being used by the microorganisms degrading the organic substrate, the spatial domain is divided into six different zones: aerobic respiration, denitrification, manganese reduction, iron reduction, sulfate reduction, and methanogenesis. The microbial utilization of the electron acceptors in each of these zones is described by the stoichiometric equations shown in Table 1. For wetland sediments, effects of plants are included by adding proper source/sink terms to account for organic carbon release (e.g., litter, exudates, root turnover), oxygen release, nutrient uptake (e.g., nitrogen), and evapotranspiration-induced advection. It is assumed here that sedimentation provides a source of fresh, bioavailable iron and manganese oxides, as well as particulate organic carbon at the sediment/water interface. For the groundwater case, a dissolved organic carbon source at the origin of the domain represents the injection of an organic substrate through a well or the leaching of biodegradable organic carbon from a source such as a landfill.

The microbial degradation of the organic matter is described by a Monod-type formulation. Reactions such as oxygen consumption by reduced compounds (e.g., Mn^{2+} , Fe^{2+} , HS^-) are formulated as second-order reactions, and precipitation of Mn^{2+} , Fe^{2+} , with HS^- and other compounds such as phosphorus and carbonate (or dissolution of the respective mineral),

are formulated as being proportional to the degree of over- or undersaturation, as shown in the appendix. Diffusion and/or advection of different chemical species across redox boundaries, followed by mixing, will result in many additional biotic and abiotic redox reactions (e.g., abiotic reduction of MnO_2 by HS^-). The most relevant reactions for the problem at hand and typical rate coefficients have been discussed by several authors (Von Gunten and Zorbist, 1993; Matsunaga et al., 1993; Smith and Jaffé, 1998). Coefficients for the biotic and abiotic reaction rates included in the simulations are given in Table 2. The model formulation allows for an easy incorporation of additional reactions that are identified as being important. Although none of the systems simulated are close to reaching chemical equilibrium conditions, the pE at a specific location is approximated to that of the dominant redox couple (Morel and Hering, 1993). The dominant redox couple in each sediment layer is assumed to be given by the half reaction of the respective electron acceptor for organic matter oxidation.

With the computed concentration profiles of the oxidized and reduced electron acceptors, pE, species such as organic carbon and ammonia, and inputted values for the pH and alkalinity, we use MINTQA2 (an EPA-supported chemical speciation model) to determine the chemical speciation under equilibrium conditions for each of a set of specified chemical constituents (e.g., trace metals, metalloids, sulfides) at each location in the sediments and/or groundwater. The difference between the actual and these equilibrium concentrations determines how far from equilibrium a reaction is. Although it is not a mechanistically-based formulation, it is convenient to describe the rate at which equilibrium conditions are approached by the product of a rate constant and the gradient given by this concentration difference. This allows a consistent, dynamic formulation for species such as arsenic and all of the other species reacting with it, considering changes in oxidation state, complexation with different ligands, and precipitation. Even though this approach of coupling a transport and chemical speciation model is computationally expensive, it has the advantage of being general and allowing for the easy incorporation/substitution of additional chemical species.

Sorption of arsenate, as well as the other species simulated, onto solid organic carbon is described by a linear sorption isotherm, and sorption onto manganese and iron oxide by the double-layer surface complexation model, accounting for interactions among these species (Dzombak and Morel, 1990). The relevant reactions and respective coefficients for the sorption model are the same as in Smith and Jaffé (1998). Colloids and dissolved organic carbon may play a role in facilitating pollutant transport in

Table 2. Key biotic/abiotic reaction parameters used in the simulation

	sediments	groundwater*
Maximum specific growth rate when [yr^{-1}]		
O_2 is the electron acceptor	4.0	1.0
NO_3^- is the electron acceptor	1.5	0.04
Mn(IV) is the electron acceptor	0.2	0.01
Fe(III) is the electron acceptor	0.032	0.005
SO_4^{2-} is the electron acceptor	1.8	0.17
Half-saturation constant of [μm]		
organic carbon	100	53.85
O_2	100	20
NO_3^-	20	20
Mn (IV)	1	3.71
Fe (III)	1	3.71
SO_4^{2-}	10	10
Threshold concentrations [μm] for indicator χ_{eA}		
O_2	0.5	
NO_3^-	6	
Mn (IV)	1	
Fe (III)	5	
SO_4^{2-}	15	
Biological As reduction rate [yr^{-1}]	130 *	
Abiotic As oxidation rate [$\text{M}^{-1} \text{yr}^{-1}$]	6.0×10^6 *	
Maximum utilization rate of [yr^{-1}]		
ammonia oxidation (nitrification)	30	
aerobic methane oxidation	10	
Half-saturation constant of [μm]		
ammonia oxidation (nitrification)	30	
aerobic methane oxidation	10	
Second-order rate coefficients for the redox reactions [$\text{M}^{-1} \text{yr}^{-1}$]		
Oxidants	Reductants	
MnO_2 (s)	Fe^{2+}	1.0×10^4
MnO_2 (s)	HS^-	8.0×10^5
FeOOH (s)	HS^-	1.0×10^3
O_2 (aq)	XMn^{2+} (ads)	2.1×10^7
O_2 (aq)	XFe^{2+} (ads)	1.6×10^8
O_2 (aq)	Fe^{2+}	2.1×10^7
O_2 (aq)	Mn^{2+}	4.6
O_2 (aq)	HS^-	2.0×10^5
NO_3^-	Fe^{2+}	1.6×10^3
$[\text{SO}_4^-]_{\text{total}}$	CH_4	1.0×10^4

* based on Kallin (1999); * Newman et al., 1997b; * Scott and Morgan, 1995; all other parameters are based on Smith and Jaffé (1998)

porous media (McCarthy and Zachara, 1989; Dunnivant et al., 1992), which was not accounted for in the simulations shown here, but can be easily included by allowing for a partitioning of the relevant species between the dissolved organic carbon and the aqueous phase.

2. RESULTS

A series of simulations were conducted to compare the dynamics of arsenic in deep sediments, wetland sediments, and in groundwaters. Physical and transport parameters used in these simulations are

Table 3. Physical and transport parameters used in the simulation

	sediments	groundwater
domain length [cm]	17.5	5000
infiltration/groundwater velocity [cm yr ⁻¹]	50	2000
dispersivity [cm]	-	25
coefficient of bioturbation [cm ² yr ⁻¹]	150	-
coefficient of irrigation [cm ² yr ⁻¹]	300	-
characteristic depth of bioturbation layer [cm]	10.5	-
characteristic depth of irrigation layer [cm]	10.5	-
porosity	0.5	0.35
dry bulk density of soil [g cm ⁻³]	1.7	2.0
pH	6.75	6.5
Fe(III) deposition rate [moles cm ⁻² yr ⁻¹]	1.0 × 10 ⁻³	-
Mn(VI) deposition rate [moles cm ⁻² yr ⁻¹]	3.3 × 10 ⁻⁴	-
carbon deposition rate [moles cm ⁻² yr ⁻¹]	5.0 × 10 ³	-
evapotranspiration rate [cm yr ⁻¹]	50	-
depth of rhizosphere [cm]	8.5	-

given in Table 3. For the sedimentary environments, constant concentration boundary conditions were set for the dissolved constituents at the water/sediment interface, and constant flux conditions for the solid components. Zero gradient conditions were set for the bottom of the domain. Zero gradient boundary conditions do affect the simulated profiles near the bottom of the domain, and changes in the gradient of some profiles near the bottom of the domain can be attributed to these boundary conditions. For the groundwater simulations, upstream constant concentration boundary conditions were set, which were equal to the initial conditions for all constituents except dissolved organic carbon. The initial conditions for dissolved organic carbon were zero throughout the domain, and the boundary conditions were set to 1.25×10^{-4} M, representing a constant injection or leaching of carbon for $t > 0$. At the outflow of the domain, zero gradient boundary conditions were used for all dissolved species. In sediments as well as wetlands one might have either groundwater recharge or discharge. The results shown here will focus on groundwater recharge, or surface water entering the sediments.

We will first compare the effect of roots on the dynamics of electron acceptors and arsenic in sediments. Figures 1 and 2 show the respective deep sediment and wetland sediment profiles of electron acceptors being consumed during the degradation of organic matter, while Figs. 3 and 4 show the profiles of their corresponding reduced forms, as well as ammonia, in deep sediments and wetland sediments, respectively (methane concentration is not shown). Simulations were conducted for a series of oxygen-release and evapotranspiration rates (Kallin, 1999). For the simulations shown here, when roots are pres-

ent, oxygen is being released into the sediments at a rate of $3 \text{ g O}_2 \text{ m}^{-2} \text{ day}^{-1}$, and evapotranspiration is 50 cm yr^{-1} . Root density was assumed to decrease as a cosine function from the water/sediment interface to a depth of 8 cm. Oxygen release, as well as water uptake as a function of depth, was assumed to be proportional to the root density.

As can be seen by comparing Figs. 1 and 2, the average oxygen concentration in the rhizosphere (upper 8.5 cm) of wetland sediments is higher in comparison to that in deep sediments (no roots present). The direct result of this increased oxygen concentration can be seen in that the oxidized species (NO_3^- , Mn(IV) , Fe(III) , and SO_4^{2-}) are transported deeper into the wetland sediments before being used as an electron acceptor. Compared to deep sediments where no roots are present, for the wetland case (with roots), this results in a decrease in the concentration gradient at the water/sediment interface and increased depth of depletion. Conversely, the reduced species shown (Mn^{2+} , Fe^{2+} , and HS^-) are being produced deeper in the wetland sediments, resulting in a decreased gradient at the water/sediment interface, and hence a reduced flux of these species into the water column (see Figs. 3 and 4). It is interesting to note the very sharp Fe^{2+} peak in these profiles. Actual Fe(III) reduction occurs only at the specific depths associated with these Fe^{2+} peaks, and the rapid disappearance of the dissolved Fe^{2+} below the Fe(III) reduction zone is due to the precipitation of FeS. These Fe^{2+} profiles are extremely sensitive to the precipitation rate, and measurements of these rates under different environmental conditions are needed. For the simulations shown in this work, a precipitation rate (k_p , as defined in the appendix) of $40 \text{ M}^{-1} \text{ yr}^{-1}$ was selected (M is the molarity).

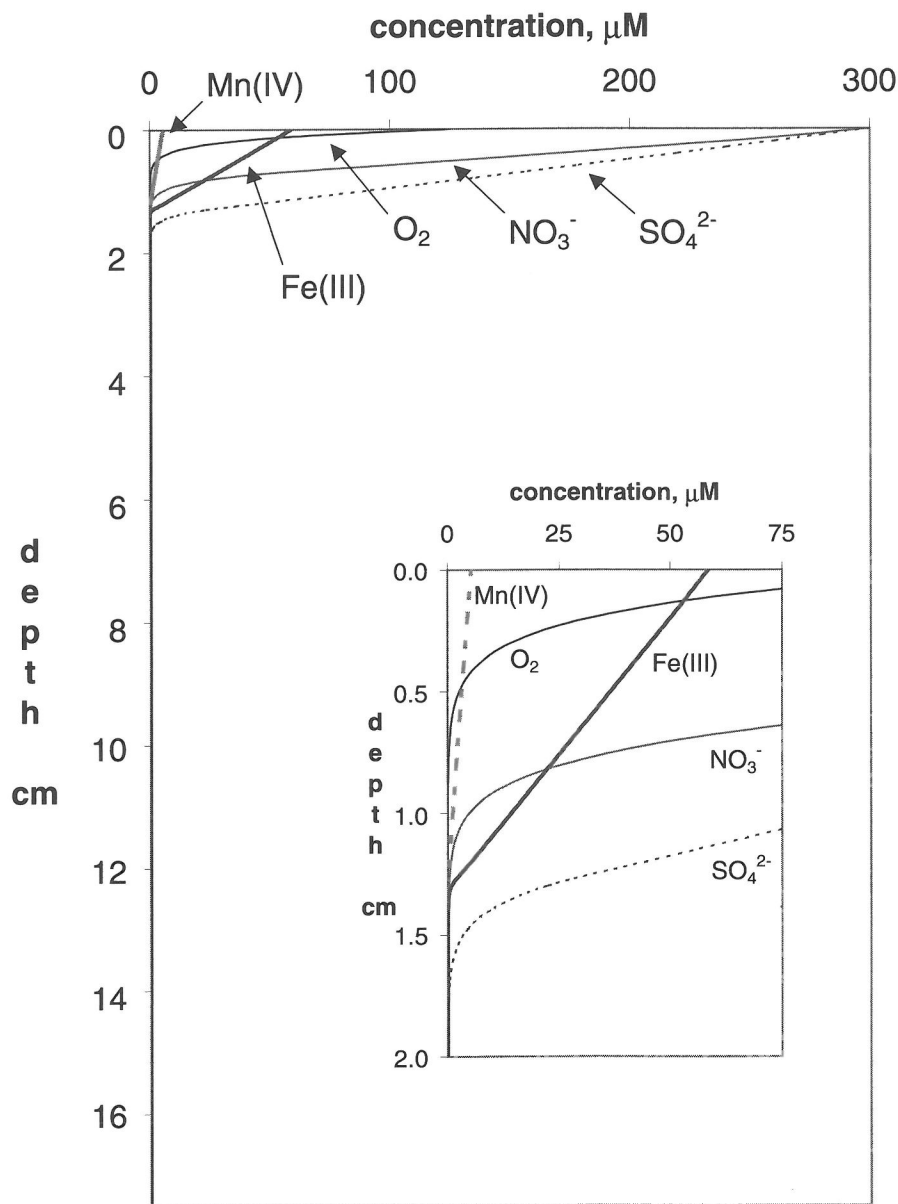


Fig. 1. Simulated concentration profiles of terminal electron acceptors in deep sediments (no roots present).

Because evapotranspiration induces flow in the sediments towards the roots, the effect of evapotranspiration on these profiles is even more marked. Evaporation-induced advection increases the flux of dissolved species (O₂, NO₃⁻, SO₄²⁻) from the water/sediment interface into the sediment. This increases the overall mass of available electron acceptors entering the sediments to the microorgan-

isms degrading the organic matter. Furthermore, since a given mass of water is withdrawn from the rhizosphere due to evapotranspiration, a mass balance for the individual species dictates that their concentrations increase due to this water withdrawal. This effect can be seen clearly for the reduced Mn, Fe, and S, which all increase in concentration throughout the whole rhizosphere, reaching concen-

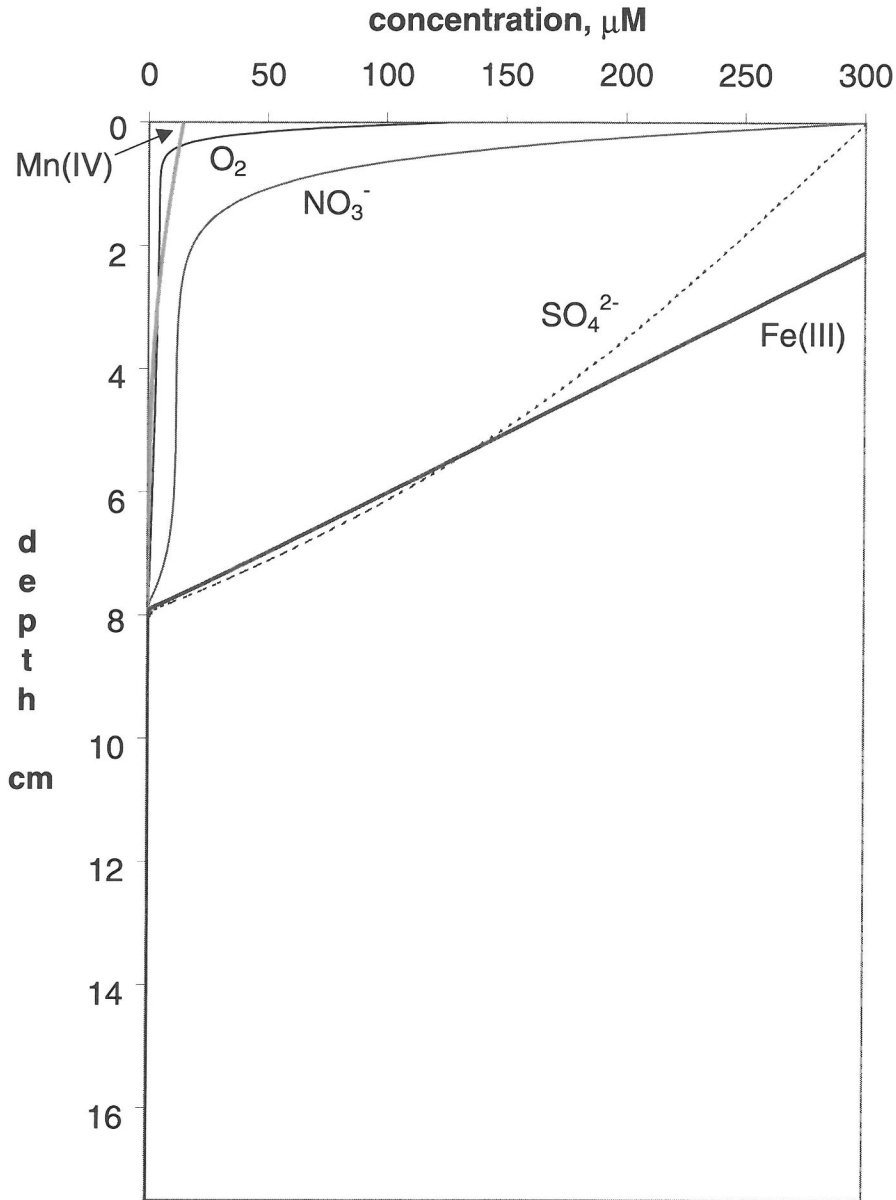


Fig. 2. Simulated concentration profiles of terminal electron acceptors in wetland sediments (roots present).

trations that are significantly higher than for the case with no roots present (compare Figs. 3 and 4).

Nitrate and ammonia uptake by plants was described by a Fickian expression, proportional to the concentration difference between the ambient concentration and a specified cutoff concentration. The nitrate and ammonia uptake rate coefficients were chosen to result in an annual biomass growth of 3,000

g/m^2 , assuming 2.5% nitrogen by weight. Additionally, sorption of NH_4^+ to the sediments was assumed to follow a linear sorption isotherm. Therefore, evapotranspiration affects the nitrate profile only in terms of increasing the overall flux into the sediments. Higher oxygen releases into the sediments by roots result in a larger conversion of ammonia into nitrate. The combined effect of increased

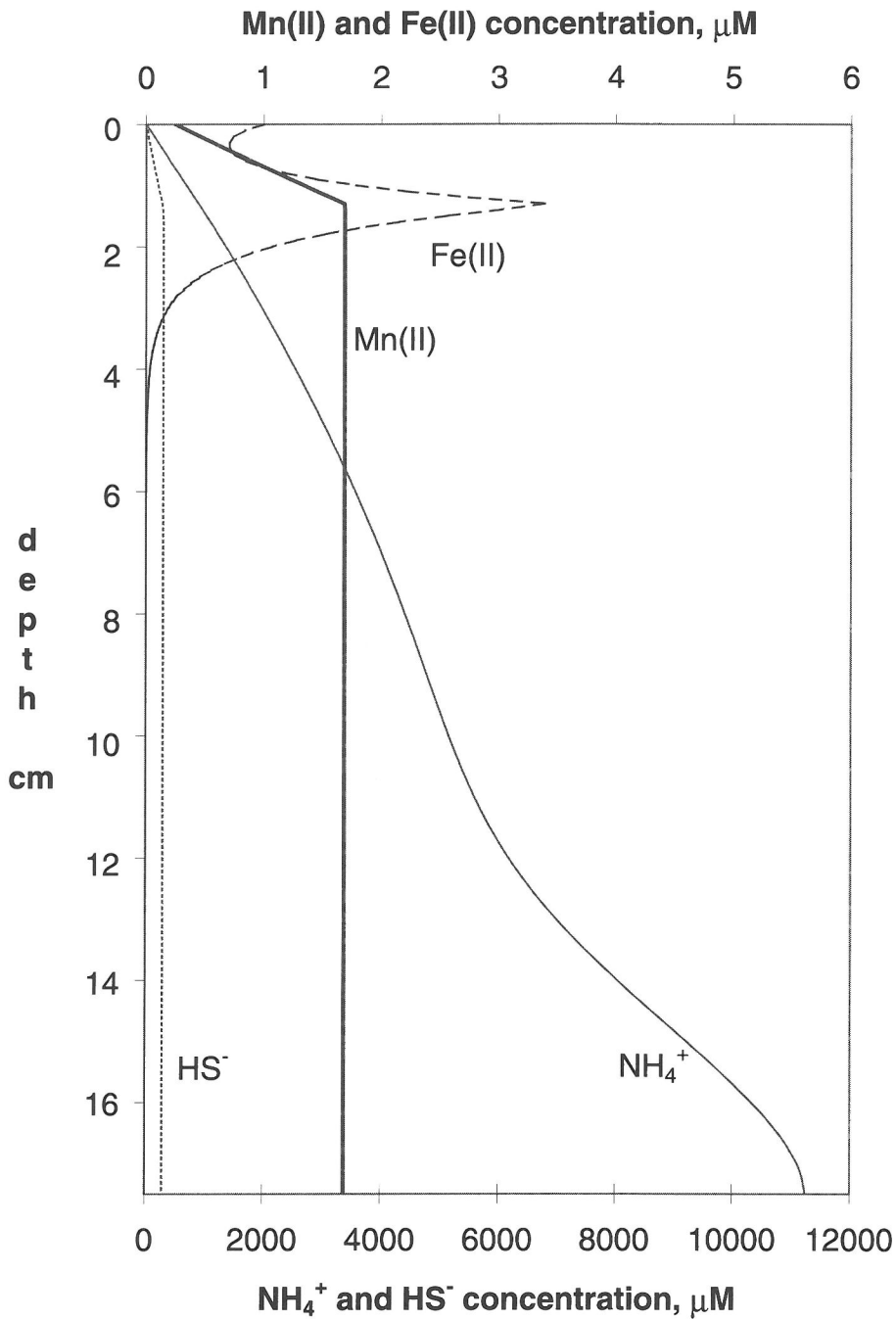


Fig. 3. Simulated concentration profiles of reduced species in deep sediments (no roots present).

nitrification and uptake by plants results in a significant decrease in the ammonia concentration in the rhizosphere of wetland sediments as compared to the deep sediment case.

Figure 5 shows the simulated profiles of dissolved arsenate and dissolved arsenite for deep sediments and wetland sediments. These profiles show that in deep sediments much steeper gradients for arsenate

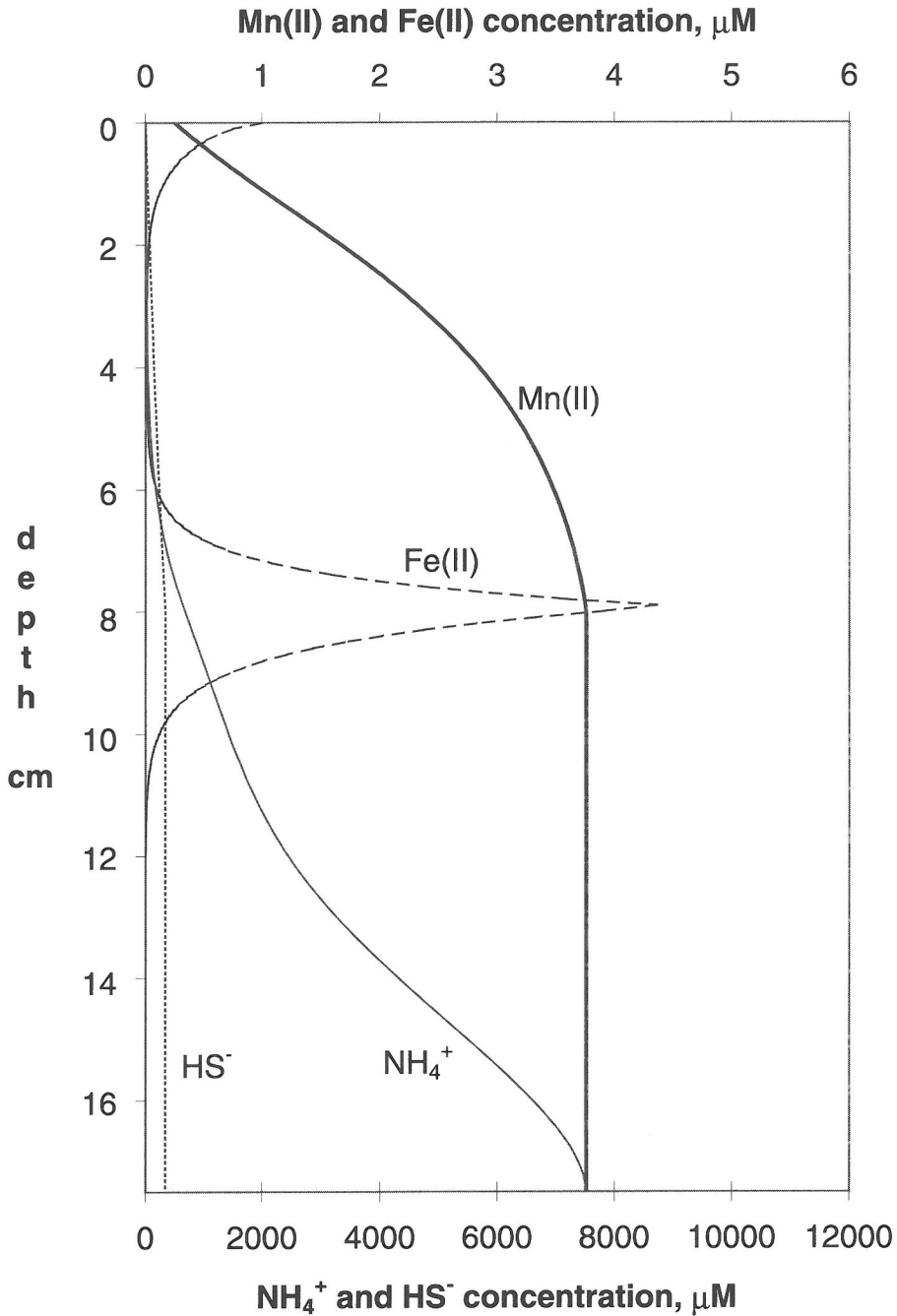


Fig. 4. Simulated concentration profiles of reduced species in wetland sediments (roots present).

and arsenite can develop at the sediment/water interface, when macrofaunal irrigation effects are not intense, as compared to the wetlands case where the profiles are less steep, due to the effects of plant roots. Therefore, a key impact of the root activity is

to decrease the flux of dissolved arsenate entering the sediments from the overlying water column, as well as the flux of the more toxic arsenite that is returned into the water column from the sediments. These fluxes are altered in their magnitude not only

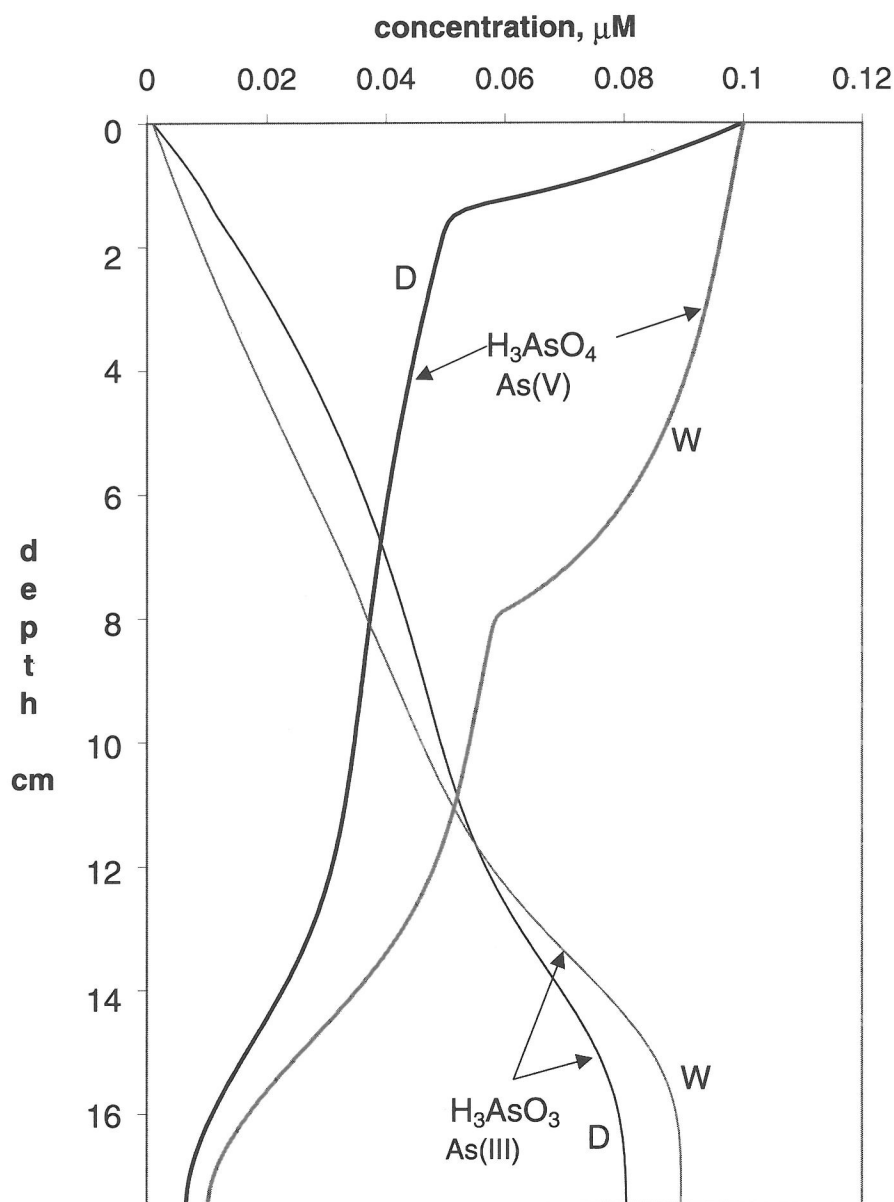


Fig. 5. Simulated concentration profiles of arsenate (As V) and arsenite (As III) in wetland (W) and deep (D) sediments.

because of the change in the concentration gradients, but also due to the increase in the advective flow induced by evapotranspiration. Since these are steady-state simulations, the dissolved-phase fluxes are not affected by the increased sorption of arsenate onto the larger amounts of iron and manganese oxides in wetland sediments. However, when the total flux of arsenic, including the sorbed phase, is

considered, the presence of plants tends to increase the amount of arsenic buried in the sediments (Kallin, 1999). If we were to consider temporal spikes in the water column's arsenic concentration, sorption would play a larger role in decreasing the dissolved-phase concentration and the effect of roots on buffering the flux of arsenite into the water column would be even larger. It should be noted that a

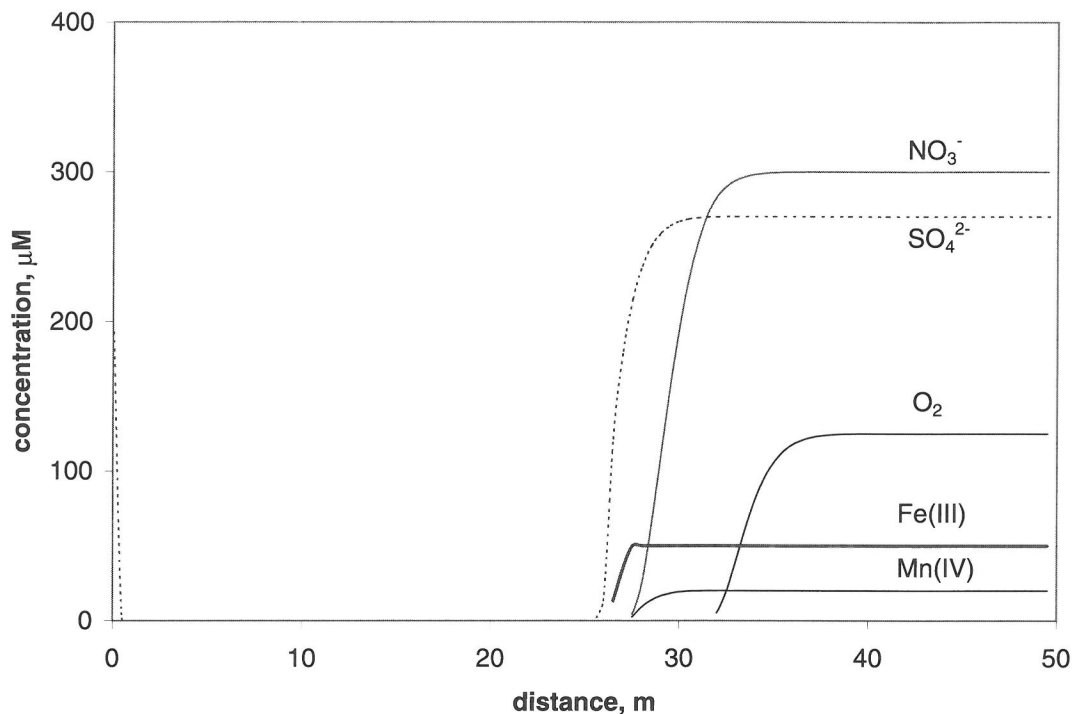


Fig. 6. Simulated concentration profiles of terminal electron acceptors in groundwater.

wide range of root density distribution can be expected, depending upon the type of wetland vegetation, and that different root density distributions will affect the individual concentration profiles.

Because of the very different nature of the groundwater environment, groundwater simulations were conducted for different flow conditions and length scales. Figure 6 shows the simulated one-dimensional profiles of the different electron acceptors, and Fig. 7 that of the reduced species, one year after a carbon source was injected at the origin. Note that in the groundwater environment the solid-phase bioavailable Mn(IV) and Fe(III) are not replenished at the interface as in the sedimentary environment, and are therefore depleted over time.

The simulated dynamics of arsenic in the groundwater environment are illustrated in Fig. 8 for time increments of 0.2 years, up to a one-year period, after a carbon source was injected at the origin. While As(V) is reduced to As(III), the total aqueous phase arsenic concentration increases significantly as time progresses. The reason for this increase is that a large fraction of the As(V) is sorbed while the As(III) sorbs to a much smaller extent. As dissolved As(V) is

reduced, sorbed As(V) will desorb to reestablish equilibrium adsorption conditions. Furthermore the ratio of dissolved to adsorbed As(V) increases over time because the bioavailable amorphous Fe(III) has been consumed as an electron acceptor, which decreases the total sites available for sorption. In these as well as in the sediment simulations, it was assumed that 30% of the total Fe(III) is amorphous and available to bacteria. Arsenate sorption to amorphous iron oxide was assumed to be the same as to the crystalline iron oxide.

As discussed earlier, arsenate can act as an electron acceptor for certain bacteria during the degradation of organic matter, and the same generic formulation was used for arsenate reduction as for the other dissolved electron acceptors. As opposed to the major electron acceptors described in the model, arsenate reduction was allowed to proceed in parallel with the reduction of the other electron acceptors after nitrate has been consumed. For this reason arsenate reduction proceeds even when the environment becomes highly reduced and methanogenesis occurs, such as deep in the sediments or in the groundwater zone where sulfate has been con-

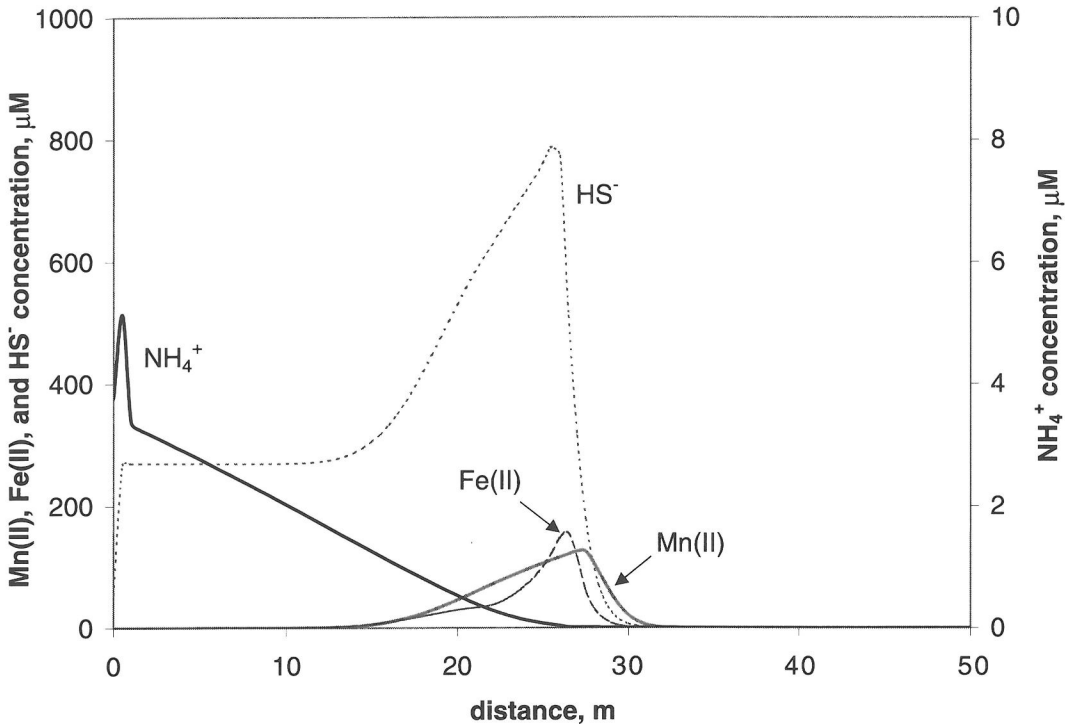


Fig. 7. Simulated concentration profiles of reduced species in groundwater.

sumed. Further research is necessary to establish if there is a lower redox limit for the reduction of arsenate. The effect of the current formulation on arsenic reduction can be seen in Figs. 5 and 8, where arsenate concentration steadily decreases and arsenite concentration increases with depth or time. Even though microbiological arsenate reduction is not initiated until all the nitrate has been consumed, Fig. 5 shows that a concentration gradient for arsenate and arsenite extends from the water/sediment interface through the aerobic and nitrate reducing zones. This gradient develops due to mixing (mainly bioturbation and irrigation) and does not imply that arsenate is being reduced in these zones. For the groundwater simulations, where there is much less longitudinal mixing, one can see clearly from Figs. 6 and 8 that after a one-year period, arsenite production is starting at the location where nitrate is depleted ($x \approx 27$ m).

3. DISCUSSION

The results presented here illustrate a methodology capable of simulating the biogeochemical dynam-

ics of trace metals and metalloids, specifically arsenic, in porous media. Redox profiles, which develop in porous media in response to the utilization of different terminal electron acceptors during the biodegradation of organic carbon, were simulated, and coupled with the dynamics of arsenic as it is transported across the different redox zones. Although there are significant differences in the formulation of physical transport processes among the three environmental settings considered here, the same generic biogeochemical formulations are applicable in all cases. The key differences in physical processes that have been considered here are sedimentation, enhanced oxygen transport by roots, transport-induced advection, and differences in mixing. We have shown that these processes have significant effects on the concentration profiles of all the chemical species simulated and how these profiles may overlap with each other. If a solid phase is being consumed, as is here the case for Mn(IV) and Fe(III), a dynamic formulation needs to be implemented if the solid matrix is stationary. For a non-stationary solid matrix, as is the case for sediments where the sediment/water interface is moving over time due to

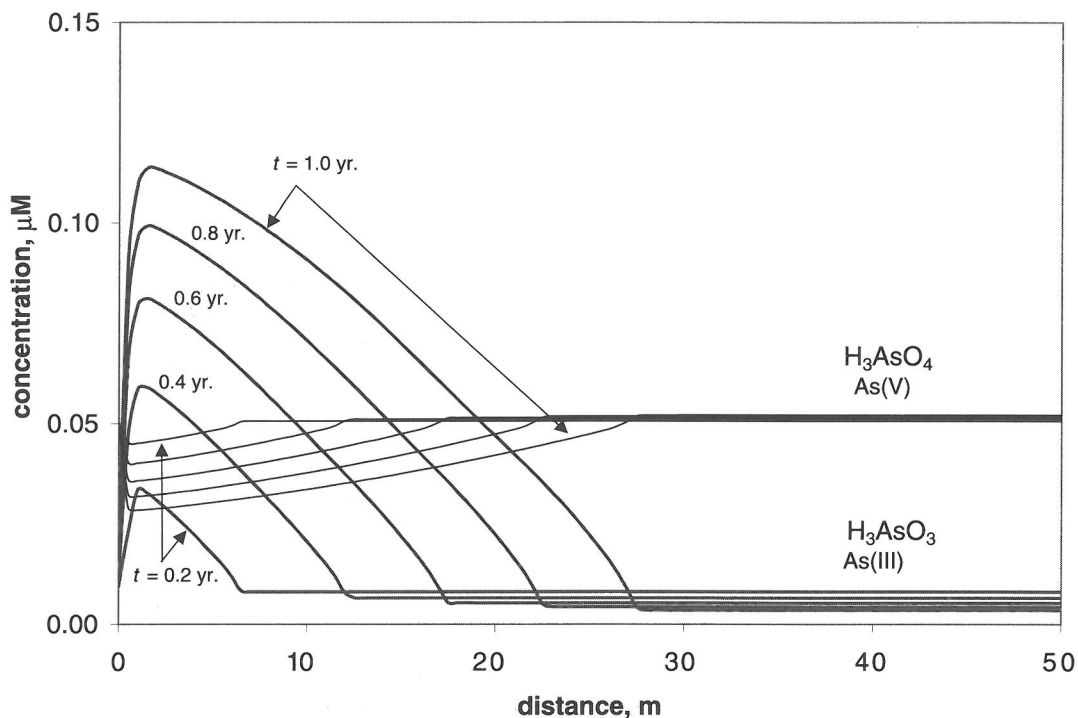


Fig. 8. Time evolution ($0.2 < t < 1.0$ yr) of arsenate and arsenite concentrations with distance in groundwater.

sedimentation, a steady-state formulation will yield zones where manganese and iron reduction are occurring. A steady-state formulation may therefore be appropriate to simulate a long-term, quasi-steady state in sedimentary environments. Given that sorption of arsenate to sorbents such as iron oxides affects the fate of arsenic in different porous media environments, it is extremely important to properly simulate the dynamics of these sorbents. Significant amounts of manganese and iron oxides can build up in the rhizosphere of wetland sediments, which can have an important effect on the overall immobilization of arsenic in wetlands.

A common feature used in the formulations examined here is that individual chemical species are not assumed to be at chemical equilibrium. Chemical equilibrium calculations are only used to determine the deviation from equilibrium conditions, based on which a kinetic formulation is implemented. This formulation allows different species to coexist. For example, as shown in all of our simulations, species such as Fe^{2+} do coexist with other more oxidized species such as NO_3^- . This

is commonly observed in sediments as well as groundwaters, and could not be simulated if equilibrium formulations were implemented.

These reaction kinetics can have significant impacts on the individual chemical profiles. As can be seen from the insert in Fig. 1, when the water flow is from the oxidized zone to the reduced zone, the electron acceptors are depleted sequentially in the order shown in Table 1. Conversely, when the water flows from reduced to more oxidized zones (e.g., groundwater for larger distances from the origin or groundwater discharge type wetlands), the various biotic and abiotic reactions occurring simultaneously can alter the spatial sequence of the profiles of the electron acceptors from that described in Table 1. This, as well as the overlapping concentration profiles near the water/sediment interface, illustrates that knowledge of the electron acceptor profiles alone does not provide adequate information to identify the zones where a specific microbiological process is occurring. Additional measurements such as the partial pressure of H_2 , which can define the bacteria capable of existing at that partial pressure (e.g.,

Lovley and Goodwin, 1988), might be required to better assess which degradation process is occurring at a given location. Such measurements may also help to more efficiently compare the accuracy of the model simulations to field data.

The simulated concentration profiles of electron acceptors in deep sediments shown here compare well to a series of profiles measured in lake sediments and described in Smith and Jaffé (1998). This was achieved using rate coefficients consistent with those reported in the literature (Smith and Jaffé, 1998; Kallin, 1999), and it therefore increases our confidence in the model. Yet accurate model verification, especially for field conditions, is difficult to achieve due to the complexity of these models and the large number of model coefficients. Even though the groundwater model formulation for the main electron donors/acceptors described here differs from that described by Hunter et al. (1998), simulations conducted for the same flow conditions and equivalent rate coefficients, resulting from either model, show a remarkably close match in the concentration profiles of the electron acceptors (not shown). This indicates that the model outputs are rather robust and not very sensitive to small alterations in the process formulations. For example, this model uses Monod kinetics for the biological reactions, while that by Hunter et al. (1998) relies on first-order kinetics.

Given the limitations in model validation, the utility of biogeochemical models such as those presented here is mainly as a scientific tool to understand variable interactions, and to be used as an aid in interpreting trends in field observations. For example, by comparing the simulations for deep sediments to those for wetland sediments, one can gain a reasonable understanding on how the colonization of aquatic plants will affect the fluxes of trace metals or metalloids in a shallow lake. Alternatively, in the case of groundwater, the simulation shows to what degree a trace metal or metalloid can be immobilized if a carbon source is added either on purpose or accidentally to the subsurface.

Finally, it should be noted that the one-dimensional models presented here do not allow for heterogeneities in the porous media where localized differences in the microbiological processes can develop. This is expected to occur in natural settings and would contribute even more to the smearing of specific concentration profiles.

Acknowledgements—The development of the model to simulate trace-metal dynamics in wetland sediments was funded in part by the U.S. EPA, grant # R827288. The simulations for arsenic in groundwater were conducted with a model devel-

oped for trace metal/radionuclide bioremediation, funded in part by the DOE NABIR program, grant # DE-FG02-98ER62705. The authors also wish to thank Drs. Nikolaidis, Van Cappellen, Charlet, and two anonymous reviewers for their constructive reviews of this manuscript.

I met David Crerar in 1982, and our first collaborative effort was on a small project dealing with the geochemistry and transport of arsenic in a shallow groundwater system. From that time, and because of David's love of nature and his wide range of interests, we had many deeply stimulating and enjoyable discussions about a variety of biogeochemical processes in different environmental settings, ranging from wetlands to lakes and groundwaters. It is for this reason that I thought this article would be appropriate in a special issue dedicated to him. I count myself fortunate to have known David as a colleague and close friend.

— Peter Jaffé
Princeton, NJ
September 2000

Editorial handling: R. Hellmann

REFERENCES

- Armstrong W. (1979) Aeration in higher plants. *Adv. Bot. Res.* **7**, 226-332.
- Bedford B., Bouldin D. R., and Beliveau B. D. (1991) Net oxygen and carbon dioxide balances in solutions bathing roots of wetland plants. *J. Ecol.* **79**, 943-959.
- Berner, R.A. (1980) *Early Diagenesis; A Theoretical Approach*. Princeton University Press, Princeton.
- Brendel, P. J. and Luther G. W. III (1995) Development of a gold amalgam voltametric microelectrode for the determination of dissolved Fe, Mn, O₂, and S(-II) in porewaters of marine and freshwater sediments. *Environ. Sci. Technol.* **29**, 751-761.
- Brix H. (1993) Macrophyte-mediated oxygen transfer in wetlands: Transport mechanisms and rates. In *Constructed Wetlands for Water Quality Improvement* (ed. G. A. Moshiri). Lewis Publishers, Inc., Boca Raton. pp. 391-398.
- Brix H., Sorrel B. K., and Schierup H. H. (1996) Gas fluxes by in situ convective flow in *Phragmites australis*. *Aquatic Botany* **54**, 151-163.
- Dhakar S. P. and Burdige D. J. (1996) A coupled, non-linear, steady state model for early diagenetic processes in pelagic sediments. *Amer. J. Sci.* **296**, 296-330.
- Dowdle P. R., Laverman A. M., and Oremland R. S. (1996) Bacterial dissimilatory reduction of arsenic(V) to arsenic(III) in anoxic sediments. *Appl. Environ. Microbiol.* **62**, 1164-1669.
- Dunnivant F. M., Jardine P. M., Taylor D. L., and McCarthy J. F. (1992) Cotransport of cadmium and hexachlorobiphenyl by dissolved organic-carbon through columns containing aquifer material. *Env. Sci. Technol.* **26**, 360-368.
- Dzombak D. A. and Morel F. M. M. (1990) *Surface Complexation Modeling: Hydrous Ferric Oxide*. John Wiley, New York.
- Egesgraad P. and Kipp K. L. (1992) A geochemical transport model for redox-controlled movement of mineral fronts in groundwater flow systems: A case of nitrate removal by oxidation of pyrite. *Wat. Resour. Res.* **28**, 2829-2843.

- Fendorf S., Eick M. J., Grossl P., and Sparks D. L. (1997) Arsenate and chromate retention mechanisms on goethite, 1. Surface structure. *Env. Sci. Technol.* **31**, 315-320.
- Gambrell R. P. and Patrick W. H. Jr. (1978) Chemical and microbiological properties of anaerobic soils and sediments. In *Plant Life in Anaerobic Environments* (eds. D. D. Hook and R. M. M. Crawford). Ann Arbor Science Publishers, Ann Arbor. pp. 375-424
- Grosse W. (1997) Gas transport in trees. In *Contributions to Modern Tree Physiology* (eds. H. Renneberg, W. Eschrich, and H. Ziegler). Backhuys Publishers, Leiden. pp. 57-74.
- Gulens J., Champ D. R., and Johnson K. E. (1979) Influence of redox environments on the mobility of arsenic in ground water. In *Chemical Modeling in Aqueous Systems*. (ed. E. A. Jenne). Amer. Chem. Soc. Symp. Ser. 93, American Chemical Society, Washington, D.C. pp. 81-95.
- Holm T. R., Anderson M. A., Iverson D. G., and Stanforth R. S. (1979) Heterogeneous interactions of arsenic in aquatic systems. In *Chemical Modeling in Aqueous Systems*. (ed. E. A. Jenne). Amer. Chem. Soc. Symp. Ser. 93, American Chemical Society, Washington, D.C. pp. 711-736.
- Hunter K. S., Wang Y., and Van Cappellen P. (1998) Kinetic modeling of microbially-driven redox chemistry of subsurface environments: coupling transport, microbial metabolism and geochemistry. *J. Hydrol.* **209**, 53-80.
- Jardine P. M., Fendorf S. E., Mayes M. A., Larsen I. L., Brooks S. C., and Bailey W. B. (1999) Fate and transport of hexavalent chromium in unsaturated heterogeneous soil. *Env. Sci. Technol.* **33**, 2939-2944.
- Kallin P. L. (1999) Modeling the fate and transport of trace metal contaminants in natural and constructed surface flow wetlands. Ph.D. thesis, Princeton University.
- Lensing H. J., Vogt M., and Herrling B. (1994) Modeling of biologically mediated redox processes in the subsurface. *J. Hydrol.* **159**, 125-143.
- Lovley, D.R. and Goodwin S. (1988) Hydrogen concentration as an indicator of the presence of the predominant terminal electron-accepting reaction in aquatic sediments. *Geochim. Cosmochim. Acta* **52**, 2993-3003.
- Massacheleyn P. H., Delaune R. D., and Patrick W.H. (1991) Effect of redox potential and pH on arsenic speciation and solubility in contaminated soil. *Environ. Sci. Technol.* **25**, 1414-1419.
- Matsunaga T., Karametaxas G., Von Gunten H. R., and Lichtner P. C. (1993) Redox chemistry of iron and manganese minerals in river recharged aquifers: A model interpretation of a column experiment. *Geochim. Cosmochim. Acta* **57**, 1691-1704.
- McCarthy J. F. and Zachara J. M. (1989) Subsurface transport of contaminants - mobile colloids in the subsurface environment may alter the transport of contaminants. *Environ. Sci. Technol.* **23**, 496-502.
- Mendelsohn I. A. (1993) *Factors controlling the formation of oxidizing root channels: a review and annotated bibliography*. Tech. Report WRP-DE-5. U.S. Army Engineer Waterways Experiment Station.
- Mitsch W. J. and Gosselink J. G. (1993) *Wetlands*, 2nd ed. Van Nostrand Reinhold Co., New York.
- Morel F. M. M. and Hering J. G. (1993) *Principles and Applications of Aquatic Chemistry*. J. Wiley & Sons, New York.
- Newman D. K., Beveridge T. J., and Morel F. M. M. (1997a) Precipitation of arsenic trisulfide by *Desulfotomaculum auripigmentum*. *Appl. Env. Microbiol.* **63**, 2022-2028.
- Newman D. K., Kennedy E. K., Coates J. D., Ahmann D., Ellis D. J., Lovley D. R. and Morel F. M. M. (1997b) Dissimilatory arsenate and sulfate reduction in *Desulfotomaculum auripigmentum* sp. nov. *Arch. Microbiol.* **168**, 380-388.
- Oscarson D. W., Huang P. M., and Liaw W. K. (1980) The oxidation of arsenite by aquatic sediments. *J. Environ. Qual.* **9**, 700-703.
- Otte M. L., Kearns C. C., and Doyle M. O. (1995) Accumulation of arsenic and zinc in the rhizosphere of wetland plants. *Bull. Environ. Contam. Toxicol.* **55**, 154-161.
- Park S. S. and Jaffé P. R. (1996) Development of a redox potential model for the assessment of postdepositional heavy metal mobility. *Ecological Modelling* **91**, 169-181.
- Ponnampuruma F. N. (1984) Effects of flooding on soils. In *Flooding and Plant Growth* (ed. T. T. Kozlowski). Academic Press, New York. pp. 10-46.
- Rabouille C. and Gaillard J.-F. (1991) A coupled model representing the deep-sea organic carbon mineralization and oxygen consumption in surficial sediments. *J. Geophys. Res.* **96**, 2761-2776.
- Sand-Jensen K., Prah C., and Stokholm H. (1982) Oxygen release from roots of submerged aquatic macrophytes. *Oikos*. **38**, 349-354.
- Scott M. J. and Morgan J. J. (1995) Reactions on oxide surfaces 1. Oxidation of As(III) by synthetic birnessite. *Environ. Sci. Technol.* **29**, 1898-1905.
- Smith S. L. and Jaffé P. R. (1998) Modeling the transport and reaction of trace metals in water-saturated soils and sediments. *Water Resour. Res.* **34**, 3135-3147.
- Sorrel B. K. (1994) Airspace structure and mathematical modelling of oxygen diffusion, aeration and anoxia in *Eleocharis sphacelata* R. Br. roots. *Aust. J. mar. Freshwater Res.* **45**, 1529-1541.
- Sorrel B. K., Brix H., and Orr P. T. (1993) Oxygen exchange by entire root systems of *Cyperus involucratu*s and *Eleocharis sphacelata*. *J. Aquatic Plant Management* **31**, 24-28.
- Sweerts J. R. A., Bar-Gillissen M.-J., Cornelese A. A., and Cappenberg T. E. (1991) Oxygen-consuming processes at the profundal and littoral sediment-water interface of a small meso-eutrophic lake (Lake Vechten, the Netherlands). *Limnol. Oceananography* **36**, 1124-1133.
- Van Cappellen P. and Wang Y. (1995) Metal cycling in sediments: Modeling the interplay of reaction and transport. In *Metal Contaminated Aquatic Sediments* (ed. H. E. Allen). Ann Arbor Press, Chelsea. pp. 21-64.
- Vitousek P.M., Fahey T., Johnson D.W., and Swift M.J. (1988) Element interactions in forest ecosystems - succession, allometry and input-output budgets. *Biogeochemistry* **5**, 7-34.
- Von Gunten U. and Zobrist J. (1993) Biogeochemical changes in groundwater infiltration systems: Column studies. *Geochim. Cosmochim. Acta* **57**, 3895-3906.
- Wang Y. and van Cappellen P. (1996) A multicomponent reactive transport model of early diagenesis: Application to redox cycling in coastal marine sediments. *Geochim. Cosmochim. Acta* **60**, 2993-3014.
- Yeh G. T. and Tripathi V. S. (1991) A model for simulating transport of reactive multispecies components: Model development and demonstration. *Water Resour. Res.* **27**, 3075-3094.

**APPENDIX — FORMULATION
OF MODEL EQUATIONS**

Mass balance equations for dissolved species

- In deep sediments:

$$\frac{\partial}{\partial t} \left(\phi [1 + K_i^{eff}] \right) C_i^{aq} = -(V - W) \frac{\partial \phi C_i^{aq}}{\partial z} + W \frac{\partial (K_i^{eff} \phi C_i^{aq})}{\partial z} + \frac{\partial}{\partial z} \left[(D_{hi} + D_b + D_{irr}) \cdot \frac{\partial \phi C_i^{aq}}{\partial z} + D_b \frac{\partial (K_i^{eff} \phi C_i^{aq})}{\partial z} \right] + \sum R_i$$

- In wetland sediments:

$$\frac{\partial}{\partial t} \left(\phi [1 + K_i^{eff}] \right) C_i^{aq} = - \frac{\partial}{\partial z} \left[(V(z) - W) \phi C_i^{aq} \right] + W \frac{\partial (K_i^{eff} \phi C_i^{aq})}{\partial z} + \frac{\partial}{\partial z} \left[(D_{hi} + D_b(z) + D_{irr}(z)) \cdot \frac{\partial \phi C_i^{aq}}{\partial z} + D_b(z) \frac{\partial (K_i^{eff} \phi C_i^{aq})}{\partial z} \right] + \sum R_i$$

- In groundwater:

$$\frac{\partial}{\partial t} \left(\phi [1 + K_i^{eff}] \right) C_i^{aq} = D_h \frac{\partial^2 \phi C_i^{aq}}{\partial x^2} - V \frac{\partial \phi C_i^{aq}}{\partial x} + \sum R_i$$

t : time [T]

ϕ : porosity

K_i^{eff} : effective partition coefficient for the equilibrium adsorption of species i [M/M]

C_i^{aq} : concentration of the dissolved species i [M/V]

V : infiltration velocity of water (positive down) in sediments or groundwater velocity [L/T]

z : distance from the sediment/water interface [L]

W : velocity of the sediment/water interface (from deposition: negative values corresponding to accumulation of sediment) [L/T]

D_{hi} : coefficient of hydrodynamic dispersion (mechanical dispersion + molecular diffusion) of species i [L²/T]

D_b : coefficient of bioturbation (mixing of sediment by aquatic and benthic organisms) [L²/T]

D_{irr} : coefficient of irrigation (mixing of porewater by benthic organisms) [L²/T]

$\sum R_i$: sum of consumption/production of species i by biotic/abiotic reactions [M/VT]

x : distance parallel to groundwater flow from the origin [L]

The effective partition coefficient for species i , K_i^{eff} , is defined as:

$$K_i^{eff} =$$

$$\frac{(1 - \phi) \cdot [\text{total adsorbed concentration of component species } i]}{\phi \cdot [\text{total dissolved concentration of component species } i]}$$

Mass balance equations for solid species

- In deep sediments:

$$\frac{\partial}{\partial t} [(1 - \phi) C_i^s] = W \frac{\partial}{\partial z} [(1 - \phi) C_i^s] + \frac{\partial}{\partial z} [(1 - \phi) D_b \cdot \frac{\partial C_i^s}{\partial z}] - \sum R_i$$

- In wetland sediments:

$$\frac{\partial}{\partial t} [(1 - \phi) C_i^s] = W \frac{\partial}{\partial z} [(1 - \phi) C_i^s] + \frac{\partial}{\partial z} [(1 - \phi) D_b(z) \cdot \frac{\partial C_i^s}{\partial z}] - \sum R_i$$

- In groundwater:

$$\frac{\partial}{\partial t} [(1 - \phi) C_i^s] = - \sum R_i$$

C_i^s : concentration of the solid species i [M/V]

The bioturbation and irrigation coefficients were assumed to decrease with depth according to:

$$D_b = \frac{D_b^0}{[1 + \exp\{z - z_b\}]}, \quad D_{irr} = \frac{D_{irr}^0}{[1 + \exp\{z - z_{irr}\}]}$$

D_b^0, D_{irr}^0 : coefficients of bioturbation and irrigation at the sediment/water interface in sediments [L^2/T],

z_b, z_{irr} : characteristic depths for bioturbation and irrigation [L]

The rate of oxidation of organic carbon, C_C , by a given terminal electron acceptor of concentration C_{eA} :

$$R_C^{eA} = -\chi_{eA} \mu_{meA} \left(\frac{C_{eA}}{K_{seA} + C_{eA}} \right) \left(\frac{C_C}{K_{seA,C} + C_C} \right)$$

χ_{eA} : indicator coefficient (1 when this electron acceptor is being utilized, and 0 when it is not)

μ_{meA} : maximum rate of carbon oxidation via this electron acceptor [M/VT]

K_{seA} : half-saturation coefficient for the electron acceptor [M/V]

$K_{seA,C}$: half-saturation coefficient for the carbon substrate (for consumption of this electron acceptor) [M/V]

The rate of consumption of a given terminal electron acceptor, which equals the rate of production of its corresponding reduced species:

$$\begin{aligned} R_{eA} &= -\alpha_{eA} \cdot R_C^{eA} = \\ &= -\alpha_{eA} \chi_{eA} \mu_{meA} \left(\frac{C_{eA}}{K_{seA} + C_{eA}} \right) \left(\frac{C_C}{K_{seA,C} + C_C} \right) \\ &= -R_{\text{corresponding reduced species}} \end{aligned}$$

α_{eA} : stoichiometric coefficient representing the ratio of the number of moles of a given electron acceptor required to oxidize one mole of organic carbon

The rate of oxidation of ammonia and corresponding production of nitrate and consumption of oxygen:

$$\begin{aligned} R_{NH_3}^{O_2} &= -\alpha_{NH_3, O_2} \mu_{mNH_3, O_2} \\ &\times \left(\frac{C_{NH_3}}{K_{s, NH_3} + C_{NH_3}} \right) \left(\frac{C_{O_2}}{K_{s, O_2}^{NH_3} + C_{O_2}} \right) = -R_{NO_3^-}^{O_2} \end{aligned}$$

Second-order rate of redox reactions:

- Rates of oxidation of dissolved reduced species i (e.g., Mn^{2+} , Fe^{2+} , HS^- , CH_4) by oxidant j :

$$R_i^j = \mu_{j,i} C_j C_i$$

$\mu_{j,i}$: second order rate coefficient

- Rates of oxidation of adsorbed Fe(II) and Mn(II) (represented as a function of the concentration of the reduced metal adsorbed onto Mn(IV) oxides):

$$R_{M^{2+}}^{ox} = \mu_{M^{2+}}^{ox} [XO_2 \cdot M^{2+}] \cdot C_{O_2}$$

$\mu_{M^{2+}}^{ox}$: rate coefficient for oxidation of adsorbed metal M^{2+}

$[XO_2 \cdot M^{2+}]$: concentration of metal M^{2+} adsorbed onto metal oxides, XO_2 (the adsorption is calculated by the equilibrium speciation model)

For a given solid, S , composed of N_s species, the net rate of precipitation, R_S^{net} :

$$R_S^{net} = k_s \cdot \left(\prod_i^{N_s} [FIA_i]^{\alpha_{i,s}} - K_{sp}^S \right)$$

k_s : precipitation rate coefficient specified for solid S [reaction dependent, for $N_s = 2$ and $\alpha_{i,s} = 1$, $M^{-1}VT^{-1}$]

FIA_i : dissolved free ion activity of component i [M/VT]

$\alpha_{i,s}$: stoichiometric coefficient of the i -th component of solid S

K_{sp}^S : equilibrium solubility product for solid S [reaction dependent, for $N_s = 2$ and $\alpha_{i,s} = 1$, M^2/V^2]

Integration of the role of plants in wetland sediment model

- Variable velocity field (described as the superposition of a groundwater infiltration velocity field and an evapotranspiration-induced velocity field)

$$V(z) = V_{inf} + \alpha ET \cdot w(z)$$

V_{inf} : groundwater infiltration velocity [L/T]

α : proportionality constant (typically assumed as 0.5)

ET : total annual evapotranspiration [L/T]

$w(z)$: a normalized root density function

$$= \cos \left[\frac{\pi}{2} \cdot \frac{z}{z_{rhiz}} \right]$$

z_{rhiz} : depth of the rhizosphere [L]

• Oxygen diffusion in the rhizosphere:

$$Oxysource(z) = \delta \cdot \frac{a}{z_{rhiz}} \cdot Rhizload \cdot w(z)$$

δ : an indicator function (1 when $z < z_{rhiz}$, 0 otherwise)

a : normalization factor

$Rhizload$: the oxygen loading [M/L²T]

• Nitrogen uptake:

$$Nitup(z) = \delta \cdot ET \cdot w(z) NitMT_0 \left(C_0^{NO_3} - C^{NO_3}(z) \right)$$

$Nitup(z)$: nitrate uptake rate [M/VT]

$NitMT_0$: baseline mass transfer rate coefficient [1/T]

$C_0^{NO_3}$: specified minimum nitrate concentration below which uptake stops [M/V]

$C^{NO_3}(z)$: aqueous nitrate concentration [M/V]

